Materials Science & Engineering A 702 (2017) 81–86

Contents lists available at ScienceDirect

Materials Science & Engineering A

journal homepage: www.elsevier.com/locate/msea

Grain boundary instability dependent fatigue damage behavior in nanoscale gold films on flexible substrates

X.M. Luo, G.P. Zhang*

Shenyang National Laboratory for Materials Science, Institute of Metal Research, Chinese Academy of Sciences, 72 Wenhua Road, Shenyang 110016, PR China

ARTICLE INFO

Keywords:
Grain growth
Thin film
Nanocrystalline
Fatigue
Damage

ABSTRACT

Quantitative investigation was performed to understand effects of length scales (film thickness) on grain growth and corresponding fatigue damage behaviors in the nanocrystalline Au thin films on flexible substrates with a film thickness ranging from 930 nm to 20 nm. In thicker films ($h \geq 90$ nm), abnormal grain growth happened due to the local high stress, while in thinner films uniform grain growth occurred. Such length–dependent grain growth mechanisms was found to be associated with the film strength and the film thickness. Consequently, the main damages in thicker films exhibited the applied load range-related competition between the intergranular cracks and the intragranular cracks along the localized slip. In the thinner film, fatigue damage is associated with GB-related behaviors, such as intergranular cracking and deformation twinning.

1. Introduction

In recent years, flexible and/or stretchable electronics have become a major research trend [1–3]. In a real application, the systems may be subjected to repeatedly mechanical deformation. For example, wearable devices will be bent, twisted and stretched repeatedly in daily use [3,4]. One of the weakest components in the system against repeatedly mechanical deformation (or fatigue loading) is a metal film, which is used as an electrical connection between electronic units [1,3]. Thus, understanding of deformation and failure mechanisms of metal films on flexible substrates under cyclic loading is a key to build high-performance and long-term reliable flexible circuits.

A cyclically deformed metal film on a substrate shows quite different deformation behaviors from its bulk counterpart [5,6], among which one of the most prominent is the length-scale-controlled fatigue behavior. Systematic investigations of the fatigue behavior of metal films on substrates reveal that when decreasing the film thickness from several microns to the submicron scale, the typical surface damage in fatigued bulk metals, such as extrusions and cracks near extrusions, is gradually suppressed and replaced by damage that is localized at interfaces [6–12]. Furthermore, when the film thickness and/or grain size decreases down to the nanoscale, grain boundary (GB) instability under cyclic loading is frequently observed in Ni [13], Cu [14] and Ni-Fe alloy [15,16], Cu films [17], Au films [18,19], Al films [20], Pd films [21], etc. Cyclic deformation behaviors have been found to be greatly affected by the microstructure instability [16,22–24]. Evident effects of cyclic softening during cyclic deformation are related to dynamic grain growth in the ultrafine-grained metals [22,25,26]. The abnormally coarsened grains frequently lead to cyclic strain localization which would accelerate fatigue damage accumulation and decrease the fatigue resistance [25,27]. However, whether the grain growth behavior is related to length scales (film thickness) and how it would affect the fatigue behaviors are still not understood well.

In the present study, a systematic investigation on grain growth and fatigue damage behaviors was performed on nanocrystalline (NC) Au films with a thickness ranging from 20 nm to 930 nm. Through the quantitative evaluation of cyclic loading-induced grain growth and the microstructure evolution in NC Au thin films, the effect of length scales on grain growth and its effect on the fatigue damage behavior were elucidated.

2. Experimental

2.1. Materials

We deposited Au films (target purity: 99.99%) with a thickness of 930 nm, 170 nm, 90 nm, 40 nm and 20 nm onto 125 μm-thick polyimide (Dupont Kapton®) substrates using DC magnetron sputtering (Denton sputtering system) under ultra-high vacuum (10^{-7} Torr) with the working pressure of 0.4 Pa. Before the deposition, the substrate was cleaned by sputtering Ar ions for about 5 min to remove the surface contamination and to improve the bond between the substrate and the film.

* Corresponding author.
E-mail address: gpzhang@imr.ac.cn (G.P. Zhang).

http://dx.doi.org/10.1016/j.msea.2017.07.006
Received 11 May 2017; Received in revised form 1 July 2017; Accepted 3 July 2017
Available online 04 July 2017

2.2. Structural characterization

X-ray diffraction (XRD) $\theta-2\theta$ scans were recorded on a Rigaku X-ray diffractometer D/MAX–2500/PC equipped with Cu-Kα radiation (56 kV, 182 mA). X-ray diffraction $\theta-2\theta$ scans reveal that all the films have a strong {111} out-of-plane texture. Surface morphologies of the films were characterized by a field-emission scanning electron microscopy (SEM, Zeiss Supra 35) under an accelerating voltage of 20 kV. The as-deposited and fatigued samples were characterized by field-emission transmission electron microscopies (TEM, FEI Tecnai F20).

TEM samples were mechanically ground to ~30 μm in thickness, and then further thinned from the substrate side by ion milling on a precision ion polishing system (Gatan 691) at −100 °C. The average size of each grain $d = (L_1 + L_2)/2$, was determined by two vertical lengths (L_1 and L_2) of the grain measured under TEM.

2.3. Fatigue testing methods

Fatigue testing of the film samples with a gauge section of ~ 13 mm in length and 3 mm in width was performed on a microforce testing system (SHIMADZU, MMT-101NV-10). Fatigue tests were performed under load control with a load ratio (the minimum load/the maximum load) of 0.1. Since the polyimide substrate is elastic and much thicker than the Au film, a constant total strain range ($\Delta\varepsilon$) can be achieved by applying such a constant load range [7,8]. Loading frequencies of the low applied load range ($\Delta\varepsilon < \sim 1.3\%$) and the high applied load range ($\Delta\varepsilon \geq \sim 1.3\%$) were 20 Hz and 1 Hz, respectively. A real-time electrical resistance (R) of the film was measured during fatigue testing to determine the fatigue life. The relative resistance increase $\Delta R/R_0 = (R - R_0)/R_0$ is correlated with the nucleation and propagation of cracks in the film [28,29]. Fatigue life (N_f), the number of cycles to failure, is determined to be cycles at which $\Delta R/R_0$ increases to 10%, where the macrocrack starts to propagate, resulting in the failure of the film (the experimental details can be found in our earlier work [29]). Besides, the reason for choosing a different fatigue frequency (1 Hz) under the high applied load range is that the resistance measurement was very unstable under the high applied load range with the frequency of 20 Hz. However, the difference in such testing frequencies in our experiment did not cause a decisive change in our conclusion, because the main conclusion is based on the comparison of experimental results under the same testing frequency. Furthermore, there are two important parameters for fatigue testing, i.e. N_f and $\Delta\varepsilon$, as shown in Fig. 1. To achieve the same N_f, thinner films would be subjected to higher applied load ranges. In this study we compared films with different thicknesses under approximately close N_f, indicating that the applied strain ranges are different in films with different thicknesses. Furthermore, enhanced load ranges were performed to films with different thicknesses so as to have a comparison under approximately close $\Delta\varepsilon$.

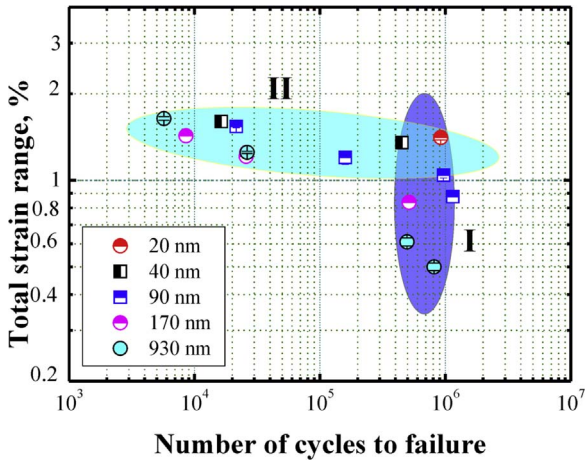

Fig. 1. Relation between applied strain range and fatigue life of the gold films. The choice of the degree of the applied load range for comparison in this study was indicated by the shadowed areas, region I and II.

3. Results and discussion

3.1. As-deposited microstructure and fatigue damage morphology

Fig. 2 shows the representative TEM images of the as-deposited Au films. The in-plan morphologies exhibit a well-equiaxed structure (Figs. 2(a)–(e)). The average in-plane grain size is in a range of several tens of nanometers and decreases with increasing the film thickness shown in Fig. 2(f).

Fatigue damage morphologies of all Au films after about 10^6 cycles mainly exhibited multiple cracks which were nearly normal to the loading direction, as shown in Fig. 3. Bulk-like fatigue extrusions/intrusions in the thicker films occurred, as indicated by the arrows in Fig. 3(b). This is quite similar to the finding in the micron-scale Cu films [12,24]. With further decreasing the film thickness to the nanometer scale, few bulk-like fatigue extrusions/intrusions could be observed, instead the directly cracking along GBs became prevailed, as shown in Fig. 3(e) and (f).

In addition to the characterization of fatigue damage behaviors, we further examined stability of nanograins in all Au films after the fatigue testing. Compared with the unfatigued samples (Fig. 2), obvious grain growth occurred in all of the fatigued samples, as shown in Figs. 4–6. Fig. 4 shows two different types of grain growth phenomena. In thicker films, abnormal grain growth occurred which is characterized by a rapid increase in size of a few grains, such that the grain size of the abnormally-grown grains is much larger than the mean [30,31], as shown in Fig. 4(a)–(f), while normal (uniform) grain growth happened, which characterized by the uniform distribution of grain size [30,31], as shown in Fig. 4(g) and (h). Obviously, when decreasing the film thickness, the grain growth tended to be locally uniform. In the following section, we will reveal the film thickness-dependent grain growth behavior and how it affected the fatigue damage behavior of the Au films on the polyimide substrate.

3.2. Grain growth and crack initiation

In the 930 nm-thick film, the fatigue damage behavior was strain-range dependent, as shown in Fig. 5. Besides, the grains obviously grew compared with that in the as-deposited film (Fig. 2(e)). Under the lower strain range ($\Delta\varepsilon$ = 0.50% and 0.61%), most fatigue cracking were along the boundaries of the uniformly grown grains, as indicated by the short arrows in Fig. 5(a) and (b). Some slip lines appeared in a few grains, as indicated by long arrows in Fig. 5(a) and (b). Such localized slip is also a preferential site for crack initiation. When increasing $\Delta\varepsilon$ = 0.84%, grains could still keep locally uniform (see Fig. 5(c)). More and more slip lines were found in individual grains. Further enhancing the applied strain range to $\Delta\varepsilon$ = 1.64%, some grains began to grow preferentially. Thus, we could observe extensive slip lines localized in those large grains, as indicated by long arrows in Fig. 5(d). The intragranular cracks initiating in the localized slip lines were the main cracking mode. When decreasing the film thickness to 170 nm and 90 nm, cracks along GBs and localized slip could also be observed, as shown in Fig. 6. However, the intragranular plasticity was obviously limited in the film with film thickness of 170 nm and 90 nm compared with that in the micron-thick film, which was evidenced by the fact that the portion of GB cracking are larger than that in the 930 nm-thick film under the similar applied strain range (see Figs. 5 and 6). When enhancing the applied strain range, some grains could also preferentially grow before the crack initiation (see Figs. 4(d) and (f)). Generally, their cracking mode was similar to the 930 nm-thick film.

When decreasing the film thickness (or grain size), the stress needed for partial dislocation nucleation (τ_p) would gradually exceed that for

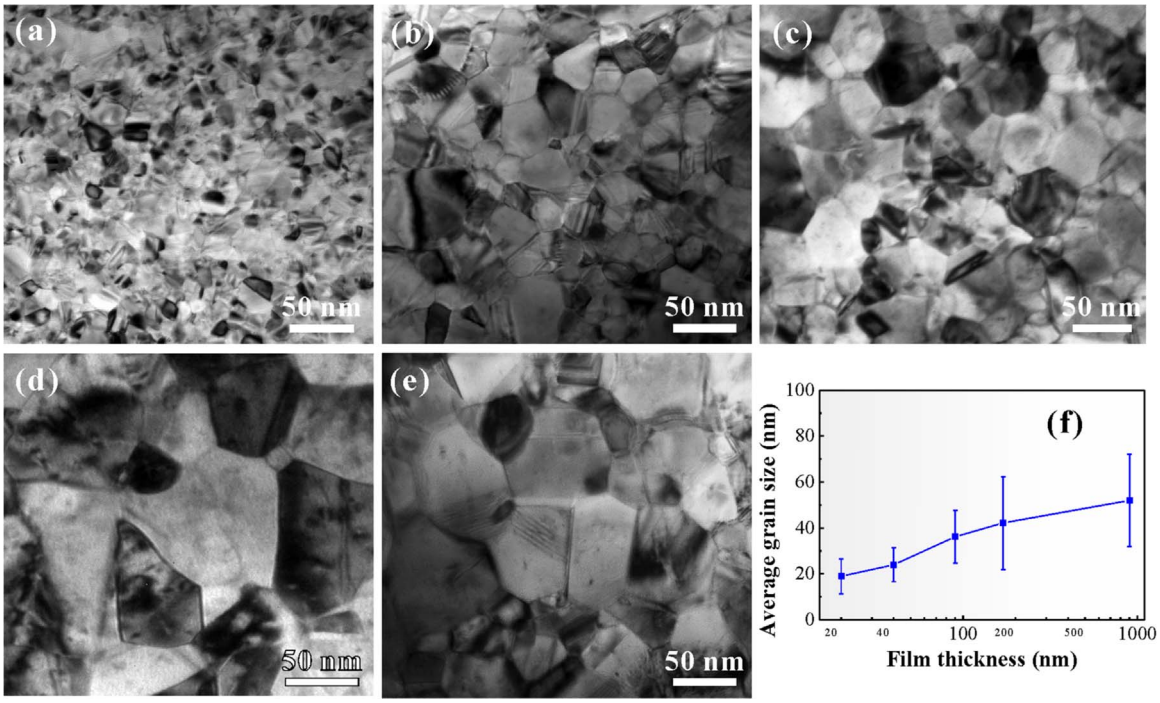

Fig. 2. In-plane TEM images of the as-deposited Au films with a thickness of (a) 20 nm, (b) 40 nm, (c) 90 nm, (d) 170 nm and (e) 930 nm. (f) Relationship between the film thickness and the average in-plane grain size in the as-deposited Au films.

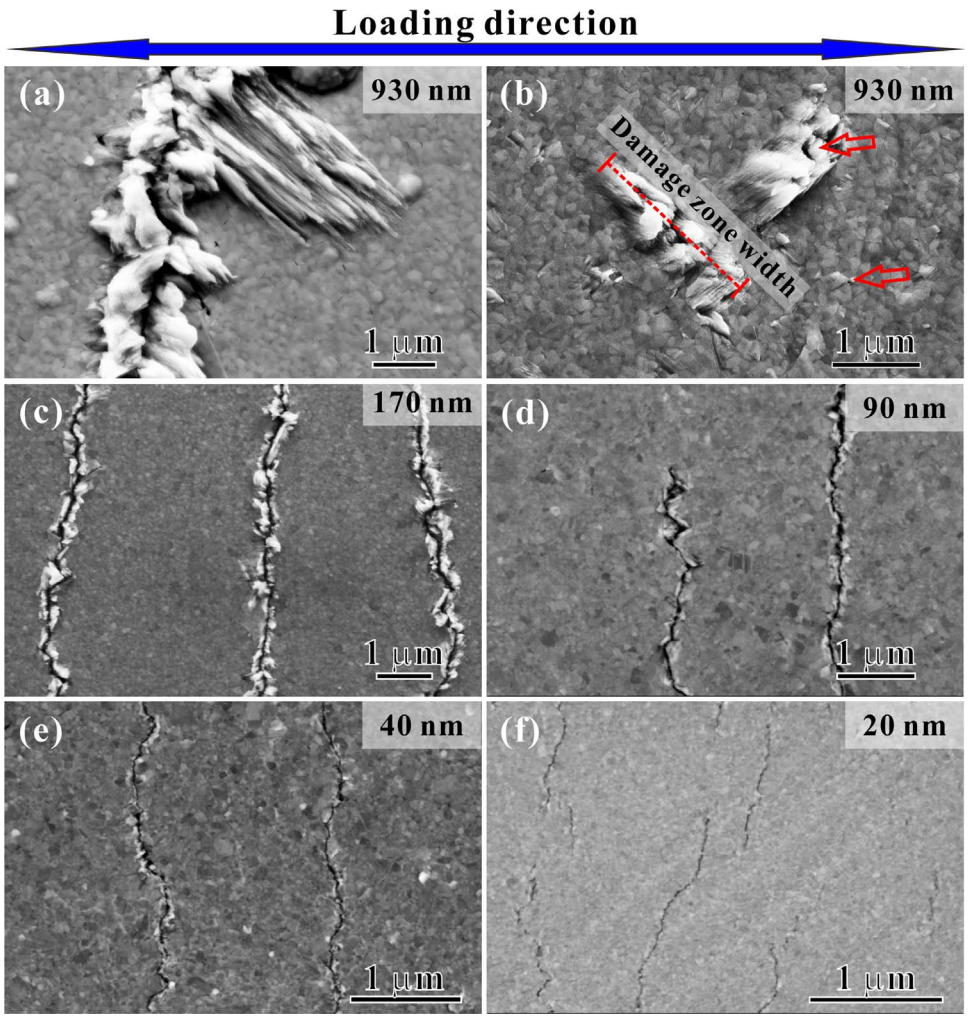

Fig. 3. SEM observation of damage morphology in Au films with a thickness of (a) 930 nm at $\Delta\varepsilon$ = 0.50%, (b) 930 nm at $\Delta\varepsilon$ = 1.64%, (c) 170 nm at $\Delta\varepsilon$ = 0.75%, (d) 90 nm at $\Delta\varepsilon$ = 0.88%, (e) 40 nm at $\Delta\varepsilon$ = 1.05%, and (f) 20 nm at $\Delta\varepsilon$ = 1.41%. The damage morphologies are mainly multiple cracks. The arrows indicate the bulk-like extrusions/intrusions with the damage zone width up to the micron scale.

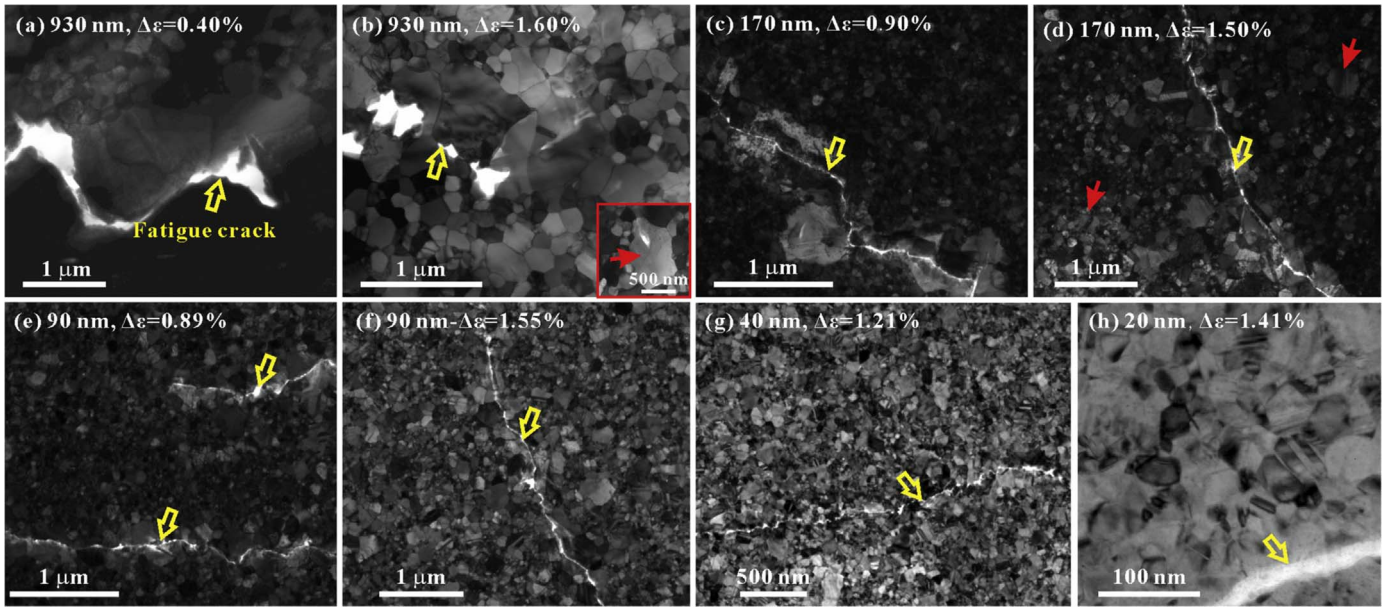

Fig. 4. TEM images of microstructures around the fatigue cracks in the films with a thickness of (a) 930 nm at $\Delta\varepsilon = 0.40\%$, (b) 930 nm at $\Delta\varepsilon = 1.60\%$, (c) 170 nm at $\Delta\varepsilon = 0.90\%$, (d) 170 nm at $\Delta\varepsilon = 1.50\%$. (e) 90 nm at $\Delta\varepsilon = 0.89\%$, (f) 90 nm at $\Delta\varepsilon = 1.55\%$, (g) 40 nm at $\Delta\varepsilon = 1.21\%$, (h) 20 nm at $\Delta\varepsilon = 1.41\%$. The inset in (b) shows the abnormally-grown grains away from the cracks. The fatigue cracks are indicated by the large open arrows. The abnormally-grown grains are indicated by the small solid arrows.

full dislocation nucleation (τ_N) [32–34], and

$$\tau_P = \frac{1}{\cos(\alpha - 30°)}\left[\frac{\sqrt{6}\gamma}{a} + \frac{Ga(1-\nu)}{8\sqrt{6}\pi(1-\nu)d}\ln\frac{\sqrt{2}d}{a}\right], \quad (1)$$

$$\tau_N = \frac{Ga}{2\sqrt{2}\pi(1-\nu)d\cos\alpha}\ln\frac{\sqrt{2}d}{a}, \quad (2)$$

where γ is the stacking fault (SF) energy, G is the shear modulus, a is the lattice parameter, ν is the Poisson's ratio, d is the grain size, and 90°-α is the angle between the shear stress and the Burgers vector. For Au [35], $\gamma = 40\ \mathrm{mJ/m^2}$, $G = 27$ GPa, $a = 0.408$ nm, $b_P = 0.166$ nm, $\nu = 0.42$, and $\alpha = 25°$. When grain size or film thickness below critical size (d_B), $\tau_P > \tau_N$, indicating that the partial dislocation behavior becomes a governing mechanism and explains the observed nanotwins. According to Eqs. (1) and (2), d_B is about 40 nm here. Thus, for the films with thickness of 40 nm and 20 nm, the full dislocation behavior is constrained by the film thickness [19]. GB-related behavior gradually takes place of the intragranular full dislocation behaviors [19,32,36–39]. Consequently, cracking along GBs becomes the main cracking mode regardless of the applied load range.

3.3. Grain growth and crack propagation

When the cracks fully propagate, the high stress at the crack tip is found to cause preferential grain growth in the films with thickness of 930 nm, 170 nm and 90 nm, where the grains are much larger than its surrounding grains, as shown in Fig. 4(a)–(f). Further decreasing the film thickness to 40 nm and 20 nm, the grain size distribution tends to be locally uniform, which means that the grain size around the fatigue crack was similar to that away from the fatigue crack, as shown in Fig. 4(g) and (h). Thus, the extent of abnormal grain growth is reduced in the thinner films.

As discussed above, the preferentially-grown grains in front of the crack tip is closely related to the high-stress level at the crack tip, thus

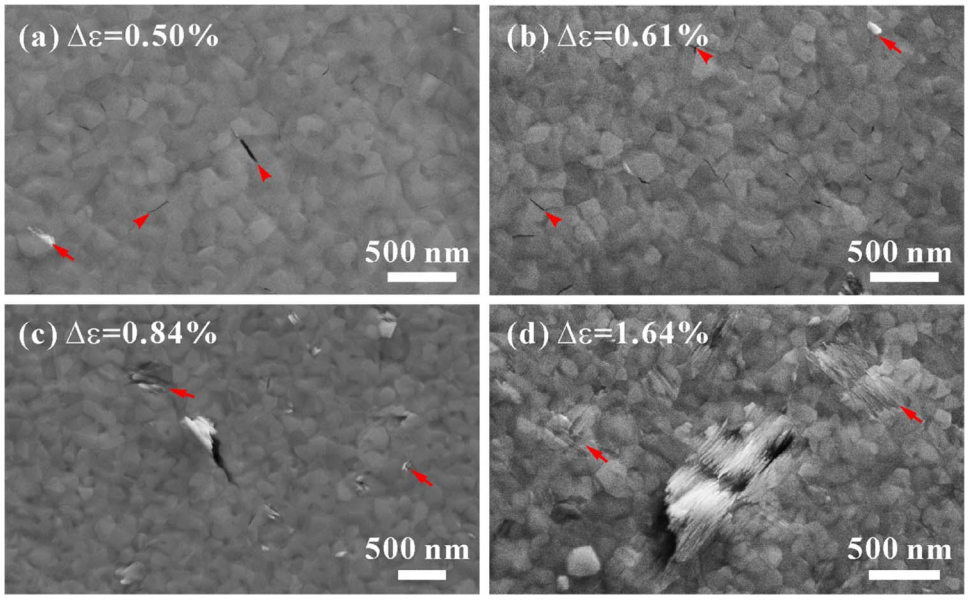

Fig. 5. SEM observation of damage morphology in 930 nm-thick Au films at (a) $\Delta\varepsilon = 0.50\%$, (b) $\Delta\varepsilon = 0.61\%$, (c) $\Delta\varepsilon = 0.84\%$, (d) $\Delta\varepsilon = 1.64\%$. The long arrows indicate the surface slip bands and the short arrows indicate the GB cracks.

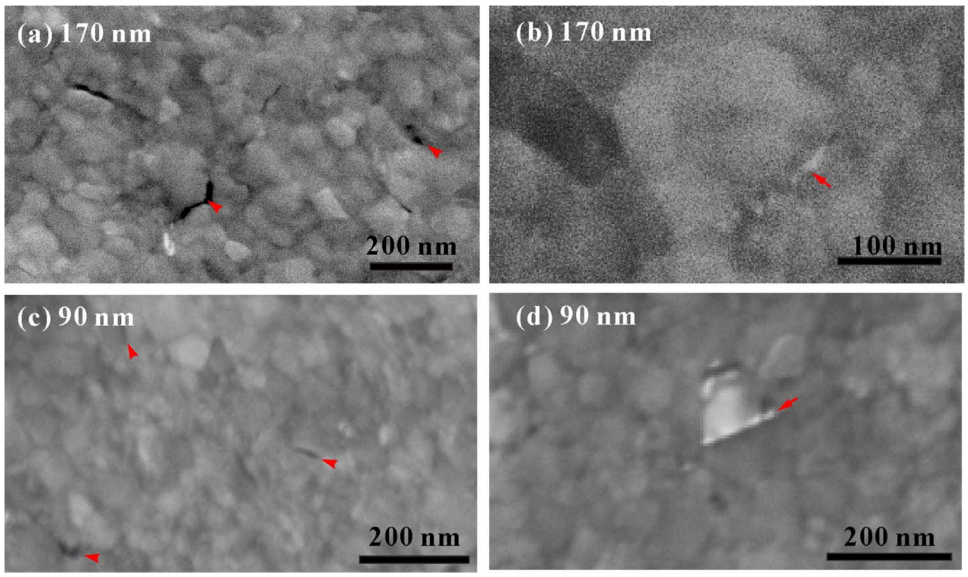

Fig. 6. SEM observation of damage morphology in Au films with a thickness of (a, b) 170 nm at $\Delta\varepsilon$ = 1.1%, and (c, d) 90 nm at $\Delta\varepsilon$ = 1.0%. The long arrows indicate the surface slip bands and the short arrows indicate the GB cracks.

we can simply estimate the size of the stress-affected zone at a channeling crack tip in the film by [40,41],

$$L_c \propto A\varepsilon_{app}^2 \cdot h \cdot \frac{1}{\sigma_y} \quad (3)$$

where A is a constant depending on material and cracking pattern, ε_{app} is the applied strain, h is the film thickness, and σ_y is the yield stress of the film. In the metal film on a substrate, the yield stress generally increases when decreasing the film thickness [42–44]. Even in the 20 nm-thick film, the twinning behavior was found to be prevailed [19,37–39,45], indicating that the relative high stress level remains in the film. Thus, the size of the stress-affected zone would decrease when decreasing the film thickness, which can simply explain the experimental results.

Overall, grain growth happened in all the films. The extent of grain growth was suggested to be associated with the applied load range, loading cycles and the film thickness, as illustrated in Fig. 7.

In thicker films ($h > \sim 90$ nm), abnormal grain growth happened along the fatigue cracks regardless of the magnitude of applied strain range, while in thinner films uniform grain growth occurred. The scaling effect on the abnormally grain growth was associated with the strength of the studied film and the film thickness.

In thicker films ($h > \sim 90$ nm): under the low applied range the main damages were intergranular cracks among the uniform grown grains, and the micron cracks gradually evolved to long cracks which would cause a considerable size of abnormally grown grains. Consequently, well-developed strain localization happened in those big grains which exhibited a bulk-like damage behavior; when enhancing the applied load range, the main damages were intergranular cracks and intragranular cracks along the localized slip in the uniform grown film. When further enhancing the applied load range, more grains were observed to exhibit localized surface sip inside the grown grains. Fatigue damage in the thinner film was associated with GB-related behaviors, such as intergranular cracking, grain coarsening as well as deformation twinning.

4. Conclusions

In summary, fatigue tests were performed on the NC Au films with a thickness ranging from 20 nm to 930 nm constrained by a polyimide substrate. We investigated the cyclic loading-induced grain growth behaviors under fatigue testing and their effects on the fatigue damage mechanisms. Grain growth happened in all the films. The extent of grain growth was suggested to be associated with the applied load range, loading cycles and the film thickness.

(1) In thicker films ($h \geq 90$ nm), abnormal grain growth happened due to the locally high stress, while in thinner films uniform grain growth occurred. Such film thickness-dependent grain growth mechanisms were suggested to be related to the size of the stress-affected zone which is dependent on the film strength and film thickness.

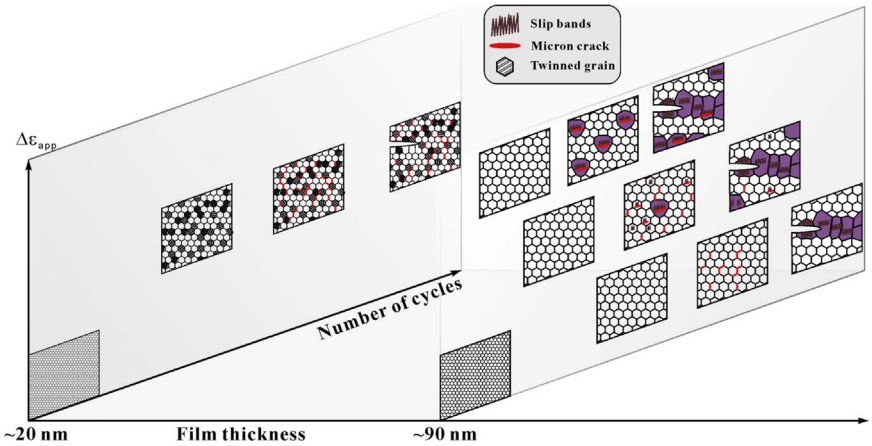

Fig. 7. Schematic illustration of the grain growth mechanisms and the corresponding fatigue damage behaviors with decreasing the film thickness and the applied strain range ($\Delta\varepsilon_{app}$).

(2) The main damages in thicker films exhibited the applied load range-related competition between the intergranular cracks and the intragranular cracks along the localized slip. When the micron cracks evolved to long cracks which would cause a considerable size of the high stress-driven abnormally-grown grains. Thus, well-developed strain localization happened in those big grains which exhibited a bulk-like damage behavior.
(3) In the thinner film, fatigue damage is associated with GB-related behaviors, such as intergranular cracking and deformation twinning.

To date, studies of the mechanical behavior of NC metal films have concentrated on scaling effect on the deformation mechanisms with decreasing the film thickness. The results reported here focus on the scaling effect of the grain growth and its effect on the fatigue damage mechanisms. Our understanding of the observed grain growth behavior and mechanisms may provide a potential clue to improve the fatigue resistance of the NC films through controlling grain growth behaviors.

Acknowledgements

This work was supported by the National Natural Science Foundation of China (NSFC, Grant nos. 51601198 and 51571199) and partially supported by the Joint Foundation of Liaoning Province National Science Foundation and Shenyang National Laboratory for Materials Science (2015021005) and the NSFC (Grant no. 51371180).

References

[1] Y.S. Rim, S.H. Bae, H. Chen, N. De Marco, Y. Yang, Recent progress in materials and devices toward printable and flexible sensors, Adv. Mater. 28 (22) (2016) 4415–4440.
[2] B. Zhu, H. Wang, W.R. Leow, Y. Cai, X.J. Loh, M.Y. Han, X. Chen, Silk fibroin for flexible electronic devices, Adv. Mater. 28 (22) (2016) 4250–4265.
[3] P. Heremans, A.K. Tripathi, A. de Jamblinne de Meux, E.C. Smits, B. Hou, G. Pourtois, G.H. Gelinck, Mechanical and electronic properties of thin-film transistors on plastic, and their integration in flexible electronic applications, Adv. Mater. 28 (22) (2016) 4266–4282.
[4] J.A. Rogers, T. Someya, Y. Huang, Materials and mechanics for stretchable electronics, Science 327 (5973) (2010) 1603–1607.
[5] R. Schwaiger, G. Dehm, O. Kraft, Cyclic deformation of polycrystalline Cu films, Philos. Mag. 83 (6) (2003) 693–710.
[6] B.-J. Kim, H.-A.S. Shin, J.-H. Lee, T.-Y. Yang, T. Haas, P. Gruber, I.-S. Choi, O. Kraft, Y.-C. Joo, Effect of film thickness on the stretchability and fatigue resistance of Cu films on polymer substrates, J. Mater. Res. 29 (23) (2014) 2827–2834.
[7] O. Kraft, R. Schwaiger, P. Wellner, Fatigue in thin films: lifetime and damage formation, Mater. Sci. Eng. A A319–321 (2001) 919–923.
[8] O. Kraft, P. Wellner, M. Hommel, R. Schwaiger, E. Arzt, Fatigue behavior of polycrystalline thin copper films, Z. Met. 93 (5) (2002) 392–400.
[9] R. Schwaiger, O. Kraft, Size effects in the fatigue behavior of thin Ag films, Acta Mater. 51 (1) (2003) 195–206.
[10] G.P. Zhang, R. Schwaiger, C.A. Volkert, O. Kraft, Effect of film thickness and grain size on fatigue-induced dislocation structures in Cu thin films, Philos. Mag. Lett. 83 (8) (2003) 477–483.
[11] R. Schwaiger, G. Dehm, O. Kraft, Cyclic deformation of polycrystalline Cu film, Philos. Mag. 83 (6) (2003) 693–710.
[12] G.P. Zhang, C.A. Volkert, R. Schwaiger, P. Wellner, E. Arzt, O. Kraft, Length-scale-controlled fatigue mechanisms in thin copper films, Acta Mater. 54 (11) (2006) 3127–3139.
[13] T. Hanlon, E.D. Tabachnikova, S. Suresh, Fatigue behavior of nanocrystalline metals and alloys, Int. J. Fatigue 27 (10–12) (2005) 1147–1158.
[14] D.C. Bufford, D. Stauffer, W.M. Mook, S.A. Syed Asif, B.L. Boyce, K. Hattar, High cycle fatigue in the transmission electron microscope, Nano Lett. 16 (8) (2016) 4946–4953.
[15] S. Cheng, Y.H. Zhao, Y.M. Wang, Y. Li, X.L. Wang, P.K. Liaw, E.J. Lavernia, Structure modulation driven by cyclic deformation in nanocrystalline NiFe, Phys. Rev. Lett. 104 (25) (2010) 255501.
[16] T.A. Furnish, B.L. Boyce, J.A. Sharon, C.J. O'Brien, B.G. Clark, C.L. Arrington, J.R. Pillars, Fatigue stress concentration and notch sensitivity in nanocrystalline metals, J. Mater. Res. 31 (06) (2016) 740–752.
[17] N. Lu, X. Wang, Z. Suo, J. Vlassak, Failure by simultaneous grain growth, strain localization, and interface debonding in metal films on polymer substrates, J. Mater. Res. 24 (02) (2011) 379–385.
[18] B. Merle, M. Goeken, Bulge fatigue testing of freestanding and supported gold films, J. Mater. Res. 29 (2) (2014) 267–276.
[19] X. Luo, X. Zhu, G. Zhang, Nanotwin-assisted grain growth in nanocrystalline gold films under cyclic loading, Nat. Commun. 5 (2014).
[20] R.R. Keller, R.H. Geiss, N. Barbosa, A.J. Slifka, D.T. Read, Strain-induced grain growth during rapid thermal cycling of aluminum interconnects, Metall. Mater. Trans. A 38A (13) (2007) 2263–2272.
[21] R.A. Meirom, D.H. Alsem, A.L. Romasco, T. Clark, R.G. Polcawich, J.S. Pulskamp, M. Dubey, R.O. Ritchie, C.L. Muhlstein, Fatigue-induced grain coarsening in nanocrystalline platinum films, Acta Mater. 59 (3) (2011) 1141–1149.
[22] H. Hoppel, M. Kautz, C. Xu, M. Murashkin, T. Langdon, R. Valiev, H. Mughrabi, An overview: fatigue behaviour of ultrafine-grained metals and alloys, Int. J. Fatigue 28 (9) (2006) 1001–1010.
[23] T.A. Furnish, A. Mehta, D. Van Campen, D.C. Bufford, K. Hattar, B.L. Boyce, The onset and evolution of fatigue-induced abnormal grain growth in nanocrystalline Ni–Fe, J. Mater. Sci. 52 (1) (2016) 46–59.
[24] B.L. Boyce, H.A. Padilla, Anomalous fatigue behavior and fatigue-induced grain growth in nanocrystalline nickel alloys, Metall. Mater. Trans. A 42 (7) (2011) 1793–1804.
[25] H. Mughrabi, H.W. Hoppel, Cyclic deformation and fatigue properties of ultrafine grain size materials: current status and some criteria for improvement of the fatigue resistance, Structure and Mechanical Properties of Nanophase Materials – Theory and Computer Simulation vs. Experiment. Symposium (Materials Research Society Symposium Proceedings vol. 634), 2001, pp. B2.1.1–B2.1.12.
[26] H.W. Höppel, Z.M. Zhou, H. Mughrabi, R.Z. Valiev, Microstructural study of the parameters governing coarsening and cyclic softening in fatigued ultrafine-grained copper, Philos. Mag. A 82 (9) (2002) 1781–1794.
[27] S.Z. Han, M. Goto, J.-H. Ahn, S.H. Lim, S. Kim, J. Lee, Grain growth in ultrafine grain sized copper during cyclic deformation, J. Alloy Compd. 615 (2014) S587–S589.
[28] G.-D. Sim, S. Won, S.-B. Lee, Tensile and fatigue behaviors of printed Ag thin films on flexible substrates, Appl. Phys. Lett. 101 (19) (2012) 191907.
[29] X.M. Luo, X.F. Zhu, G.P. Zhang, Nanotwin-assisted grain growth in nanocrystalline gold films under cyclic loading, Nat. Commun. 5 (2014) 3021.
[30] M. Hillert, On the theory of normal grain growth and abnormal grain growth, Acta Metall. 13 (3) (1965) 227.
[31] D.J. Srolovitz, G.S. Grest, M.P. Anderson, Computer simulation of grain growth—V. Abnormal grain growth, Acta Metall. 33 (12) (1985) 2233–2247.
[32] Y.T. Zhu, X.Z. Liao, X.L. Wu, Deformation twinning in nanocrystalline materials, Progress. Mater. Sci. 57 (1) (2012) 1–62.
[33] Y.T. Zhu, X.Z. Liao, S.G. Srinivasan, Y.H. Zhao, M.I. Baskes, F. Zhou, E.J. Lavernia, Nucleation and growth of deformation twins in nanocrystalline aluminum, Appl. Phys. Lett. 85 (21) (2004) 5049.
[34] Y.T. Zhu, X.Z. Liao, S.G. Srinivasan, E.J. Lavernia, Nucleation of deformation twins in nanocrystalline face-centered-cubic metals processed by severe plastic deformation, J. Appl. Phys. 98 (3) (2005) 034319.
[35] S.H. Oh, M. Legros, D. Kiener, P. Gruber, G. Dehm, In situ TEM straining of single crystal Au films on polyimide: change of deformation mechanisms at the nanoscale, Acta Mater. 55 (16) (2007) 5558–5571.
[36] T.J. Rupert, D.S. Gianola, Y. Gan, K.J. Hemker, Experimental observations of stress-driven grain boundary migration, Science 326 (5960) (2009) 1686–1690.
[37] V.I. Levitas, A.M. Roy, D.L. Preston, Multiple twinning and variant-variant transformations in martensite: phase-field approach, Phys. Rev. B 88 (5) (2013) 054113.
[38] V.I. Levitas, J.A. Warren, Thermodynamically consistent phase field theory of phase transformations with anisotropic interface energies and stresses, Phys. Rev. B 92 (14) (2015) 144106.
[39] V.I. Levitas, A.M. Roy, Multiphase phase field theory for temperature-induced phase transformations: formulation and application to interfacial phases, Acta Mater. 105 (2016) 244–257.
[40] J.W. Hutchinson, Z. Suo, Mixed-mode cracking in layered materials, in: J.W. Hutchinson, T.Y. Wu (Eds.), Advances in Applied Mechanics, 29 1992, pp. 63–191.
[41] S. Suresh, Fatigue of Materials, 2nd ed., Cambridge University Press, Cambridge, 1998.
[42] O. Kraft, P.A. Gruber, R. Mönig, D. Weygand, Plasticity in confined dimensions, Ann. Rev. Mater. Res. 40 (1) (2010) 293–317.
[43] W.D. Nix, Yielding and strain hardening of thin metal films on substrates, Scr. Mater. 39 (4–5) (1998) 545–554.
[44] W.D. Nix, Mechanical properties of thin films, Metall. Mater. Trans. A 20 (11) (1989) 2217–2245.
[45] P.A. Gruber, C. Solenthaler, E. Arzt, R. Spolenak, Strong single-crystalline Au films tested by a new synchrotron technique, Acta Mater. 56 (8) (2008) 1876–1889.